

Supporting Information

On the nucleation and fast reaction kinetics of 2D polymerisation with a 2-in-1 monomer

Niklas Herrmann,^a Cristina Martin,^b Samuel Eyley,^c Yusen Li,^d Nerea Bilbao,^a Víctor R. Giménez,^e Mark Van der Auweraer,^a Wim Thielemans,^c Long Chen,^{d*} Kunal S. Mali,^{a*} and Steven De Feyter^{a*}

^a*Division of Molecular Imaging and Photonics, Department of Chemistry, KU Leuven, Celestijnenlaan 200F, 3001 Leuven, Belgium.* ^b*Department of Physical Chemistry, Faculty of Pharmacy, University of Castilla-La Mancha, 02071 Albacete, Spain* ^c*Sustainable Materials Lab, Department of Chemical Engineering, KU Leuven, Campus Kulak Kortrijk, Etienne Sabbelaan 53, 8500 Kortrijk, Belgium.* ^d*State Key Laboratory of Supramolecular Structure and Materials, College of Chemistry, Jilin University, Changchun 130012, China.* ^e*Membrane Separations, Adsorption, Catalysis, and Spectroscopy for Sustainable Solutions, Department of Chemistry, KU Leuven, 3001 Leuven, Belgium.*

Contents:

1. Materials

2. Methods

- a) *Ex-situ* 2D-COF synthesis.
- b) Scanning tunnelling microscopy (STM).
- c) UV-vis spectroscopy.
- d) Attenuated total internal reflection-infrared (ATR-IR) spectroscopy.
- e) X-ray photoelectron spectroscopy (XPS).

3. Supporting data

- a) Supporting UV-vis spectroscopy data.
-Temperature- and time-dependent UV-vis absorbance of 2-in-1 monomer (**Fig. S1**).
- b) Supporting STM data.
-STM images showing the time-dependent evolution of the 2DP at the OA-DMSO/HOPG interface (**Fig. S2**).
-Large scale STM images showing the time-dependent evolution of the 2DP at the OA-DMSO/HOPG interface (**Fig. S3**).
-STM images showing disordered networks and multilayers of 2DP formed at the at the OA-DMSO/HOPG interface (**Fig. S4**).
- c) Supporting XPS data.
-Additional XPS data showing the effect of thorough rinsing of the sample to remove residual monomers (**Fig. S5**).

4. Synthesis of structurally similar tetraaldehyde (1) and tetraamine (2)

1. Materials

Octanoic acid (Roth, 99.5%), DMSO (VWR chemicals, 99.8%, anhydrous, 0.005% water), methanol (Sigma Aldrich, for spectroscopy) and 2,5-dimethoxyterephthalaldehyde (TCI chemicals) were used as received. The 2-in-1 monomer was synthesised as described in Ref. [1], **1** and **2** (see last section for synthetic details) were synthesised according to the reported procedures in Ref. [2].

2. Methods

a) *Ex-situ* 2D COF synthesis

A DMSO/OA (50:50 V:V) solution of **1** ($c = 9 \times 10^{-4}$ M) was heated in a closed glass snap-cap vial to 90 °C for 2 h. The resulting mixture was transferred to a falcon tube and centrifuged (5 min, 800 *g*) to yield a yellow solid. The supernatant was discarded and the solid was washed with methanol twice before being dried at 70 °C to yield a yellow powder. Repeated runs of this procedure with slightly lower monomer concentrations gave additional batches of *ex-situ* COF showing the same characteristics.

b) STM

STM experiments were performed using either Keysight Pico LE or Molecular Imaging microscopes in custom-made isolation chambers at ambient conditions ($T = 20\text{--}24$ °C, humidity 30–60%) in constant current mode using mechanically cut Pt/Ir tips (80%/20%, $d = 0.25$ mm, Advent Research Materials) with the tip immersed in the supernatant liquid during the measurement. HOPG ZYB grade ($12 \times 12 \times 2$ mm, Momentive Performance Materials) was purchased from Bruker and freshly cleaved with adhesive tape prior to drop casting. Few seeding particles were taken from a batch of *ex-situ* synthesised COF and applied to the HOPG surface before drop casting. Stock solutions of the 2-in-1 monomer and compounds **1-2** ($c \approx 1\text{--}10$ mM) (*vide infra*) in DMSO were prepared and stored at room temperature until dilution to the desired concentration with OA just before drop casting. The DMSO share of the final solutions was kept below 5% (V:V). STM image analysis which included flattening and line removal was performed either using Scanning Probe Image Processor (SPIP) software (Image Metrology ApS) or Gwyddion 2.56, 2.57, 2.58, 2.59, 2.60, and 2.61.³ The STM images provided in the main text are Gaussian filtered. The imaging parameters are indicated in the figure caption: tunnelling current (I_{set}), and sample bias (V_{bias}).

c) UV-vis spectroscopy

Experiments were performed on a PerkinElmer Lambda 950 spectrometer using $d = 10$ mm glass cuvettes (Hellma Analytics SUPRASIL High Precision Cell) in transmission mode. For the kinetic experiments, the solutions ($c = 5 \times 10^{-6}$ M in OA/DMSO) were magnetically stirred inside the cuvette during the measurement. The cuvette holder was externally heated to the desired temperature for the duration of the experiment. The cuvettes were closed to prevent solvent evaporation. All solid material spectra were obtained in reflectance mode with the material held between two pieces of quartz glass.

d) Attenuated total internal reflection-infrared (ATR-IR) spectroscopy

ATR-IR measurements were performed on Py-COF powder under ambient conditions on a Bruker Vertex 70.

e) X-ray photoelectron spectroscopy (XPS)

Dry Py-COF films for XPS were prepared by drop casting of the same OA/DMSO solutions as used for STM, followed by drying in the hot air stream of a heat gun in normal atmosphere. XPS was performed on a Kratos Axis Supra photoelectron spectrometer with a monochromated Al K α (1486.7 eV, 150 W) X-ray source, hybrid (magnetic/electrostatic) optics and hemisphere analyser. The analyser was operated in fixed analyser transmission mode, with high resolution scans taken at 20 eV. All spectra were collected at normal emission, with samples in electrical contact with the spectrometer ground. Spectra were analysed using CasaXPS version 2.3.25.

3. Supporting data

a) Supporting UV-vis spectroscopy data

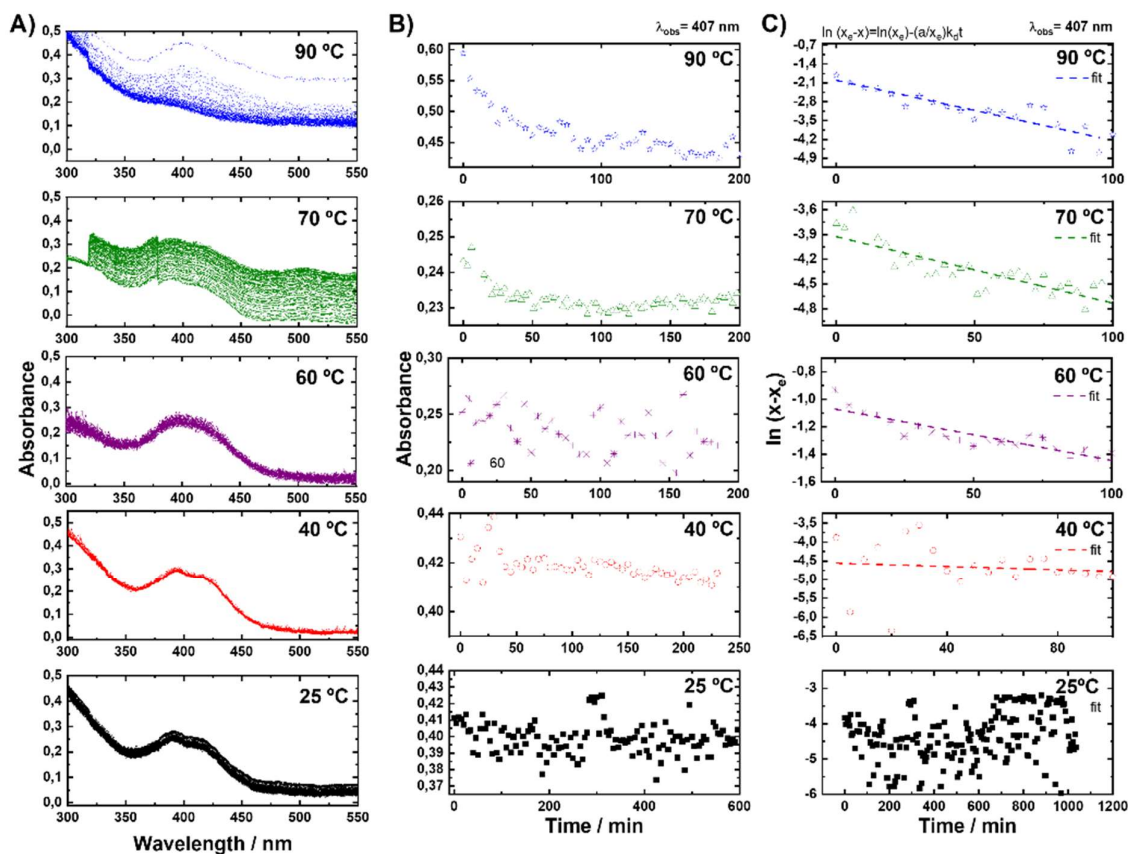


Fig. S1 Temperature- and time-dependent UV-vis absorbance of 2-in-1 monomer suspension in octanoic acid ($5 \cdot 10^{-6} \text{ M}$) (A) UV-vis absorption spectra time series at different temperatures (indicated in the spectra). (B): Time evolution of the UV-vis absorbance at 407 nm of 2-in-1 monomer suspension in octanoic acid at different temperatures (indicated in the spectra), showing a decrease in absorption over time. (C): Logarithmic fit of the absorption at 407 nm over time at different temperatures. The dashed line represents the best fit for reversible kinetics. In this equation, k_d is the reaction rate constant for the system. 25 °C (black), 40 °C (red), 60 °C (purple), 70 °C (green), and 90 °C (blue).

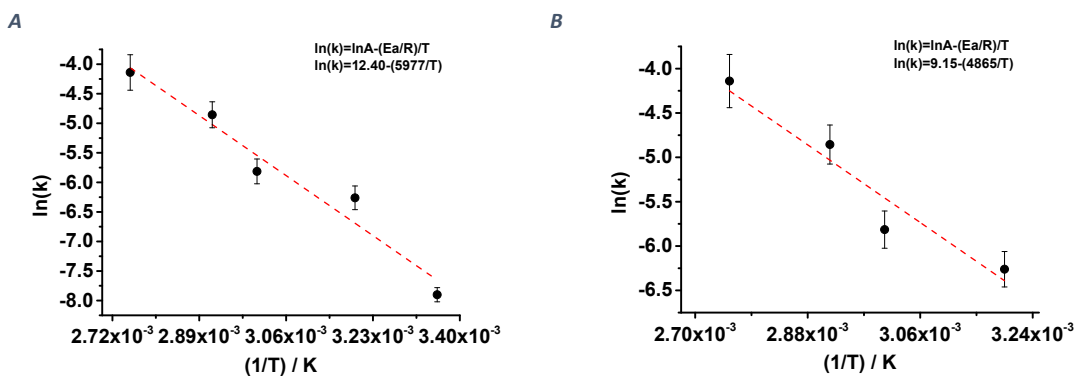


Fig. S1a. Comparison of the Arrhenius plots considering different temperature ranges. The plots reveal no significant change in activation energy ($4.5 \text{ kJ}\cdot\text{mol}^{-1}$ vs $6 \text{ kJ}\cdot\text{mol}^{-1}$). The error bars to the Arrhenius plots are taken from the error of each individual kinetic fit.

Note on the pre-exponential factor:

In this case, although formally first order, one should bear in mind that this reaction is a complex multistep process involving a catalyst (acid). This means that the overall rate constant can be a product of equilibrium constants of pre-equilibria and the actual rate constant of the rate-determining step.

In more detail, we can consider that globally the reaction is the association of monomers³ to monomers or an extension of existing COF structure by bonding an extra monomer to form an ordered 2D-COF. In such a process, the entropy of the system will be reduced. This will, whatever the exact mechanism is, lead to a negative activation entropy reducing the pre-exponential factor below values of the order of kT/h . The presence of steric constraints in the transition state will make the activation entropy more negative and further reduce the pre-exponential factor.

Further analysis of the pre-exponential factor, which is needed in order to extract a quantitative value is not straightforward as the reaction is fairly complex.

b) Supporting STM data

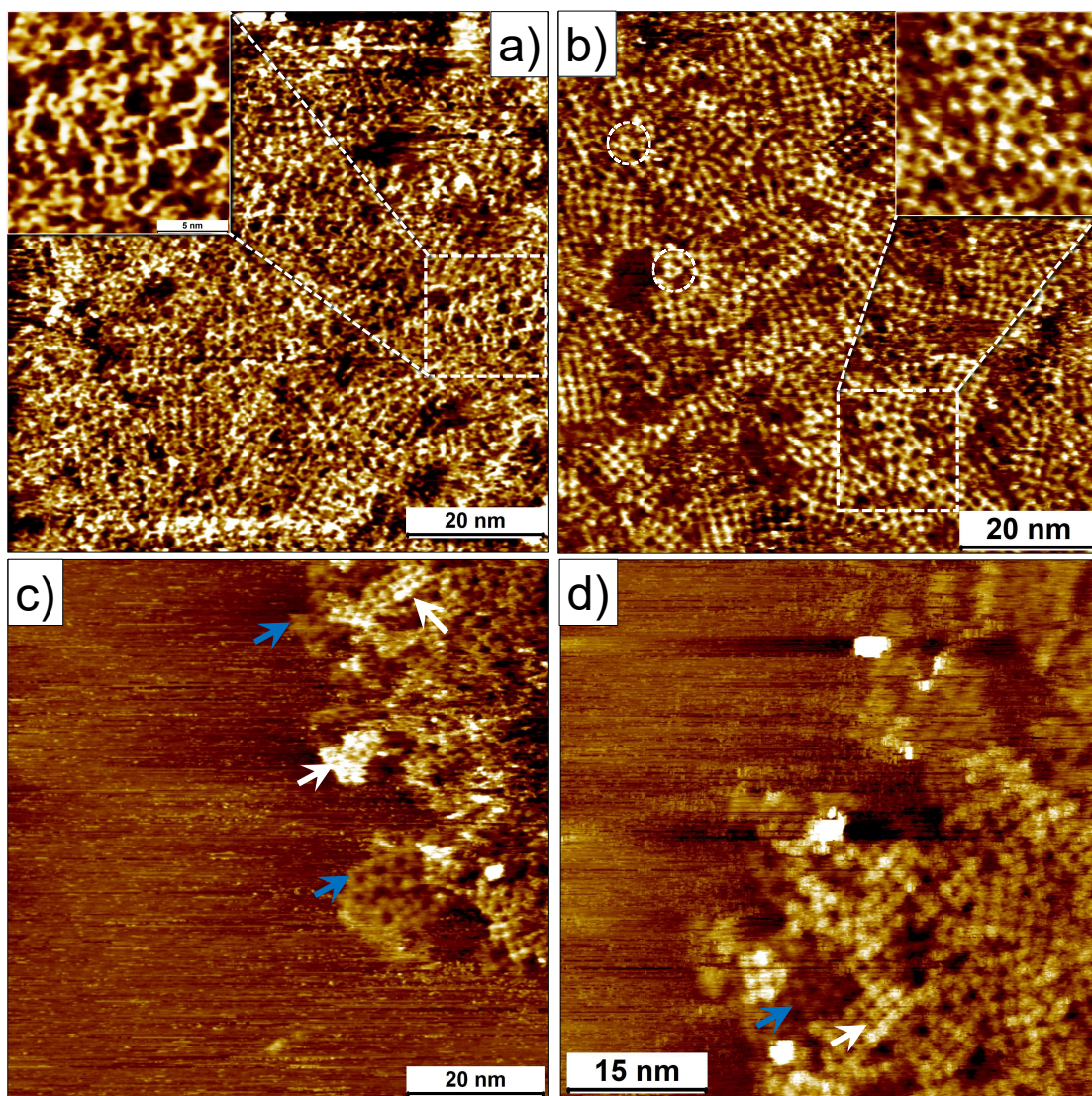


Fig. S3 STM images showing the formation of non-rectangular cavities and multilayers at the OA/DMSO-graphite interface indicating fast nucleation of the covalent structures. (a, b) STM images showing non-rectangular cavities formed due to deviation from the normal unit cell. The inset in (a) shows hexagonal structure whereas the inset in (b) shows flower-like networks. White dashed circles in (b) show triangular structures. The hexagonal structures (Fig S2a) arise from the E/Z isomerism of the imine bonds, while the irregular structures with ring sizes of $n \neq 4$ arise from the incorporation of additional monomer molecules during the initial nucleation and growth phase of the 2D COF flakes (and E/Z isomerism). (c, d) STM images showing the formation of multi-layered structures where the bottom layers (blue arrows) could be discerned from the top layers (white arrows). Concentration of the monomer was 5×10^{-5} M in OA/DMSO. Imaging parameters: (a) $V_{\text{bias}} = -0.5$ V, $I_{\text{set}} = 0.09$ nA (b) $V_{\text{bias}} = -0.4$ V, $I_{\text{set}} = 0.08$ nA (c, d) $V_{\text{bias}} = -0.6$ V, $I_{\text{set}} = 0.065$ nA.

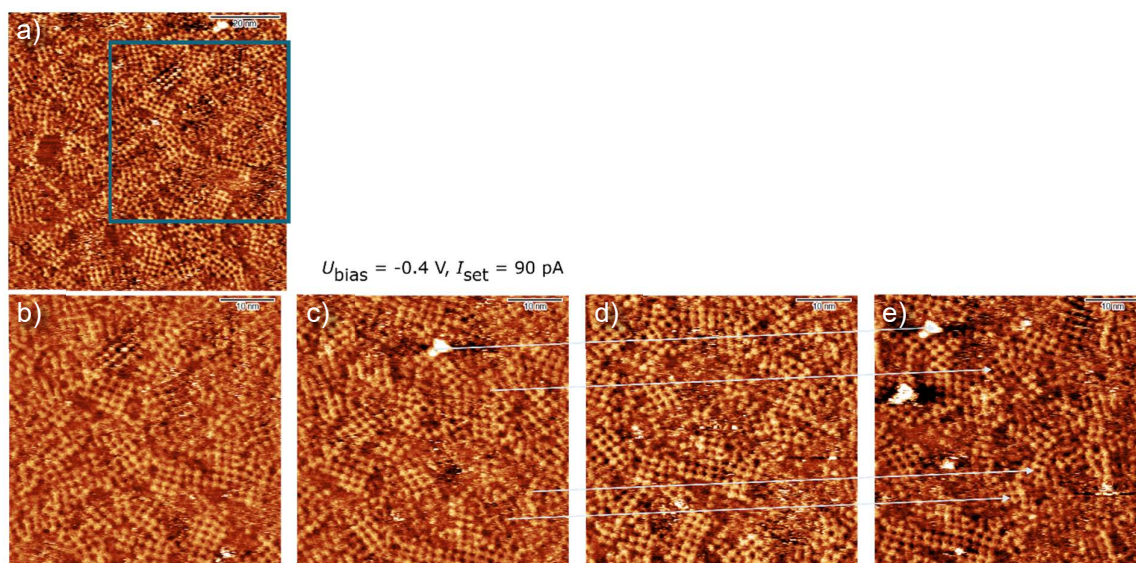


Fig. S4 Time-series of STM images of the 2-in-1 monomer at the OA-DMSO/HOPG interface, at room temperature. Concentration = $5 \times 10^{-5} \text{ M}$. Top panel: large scale STM image. Lower panels: STM images of the area within the blue rectangle at different times (from left to right), revealing negligible dynamics and growth of the 2DP domains. Defects, indicated by white arrows, are used as reference points to account for thermal drift. The imaging of a single frame took approximately 90 s. The scale bar equals 10 nm. Imaging parameters: $V_{\text{bias}} = -0.4 \text{ V}, I_{\text{set}} = 0.90 \text{ nA}$.

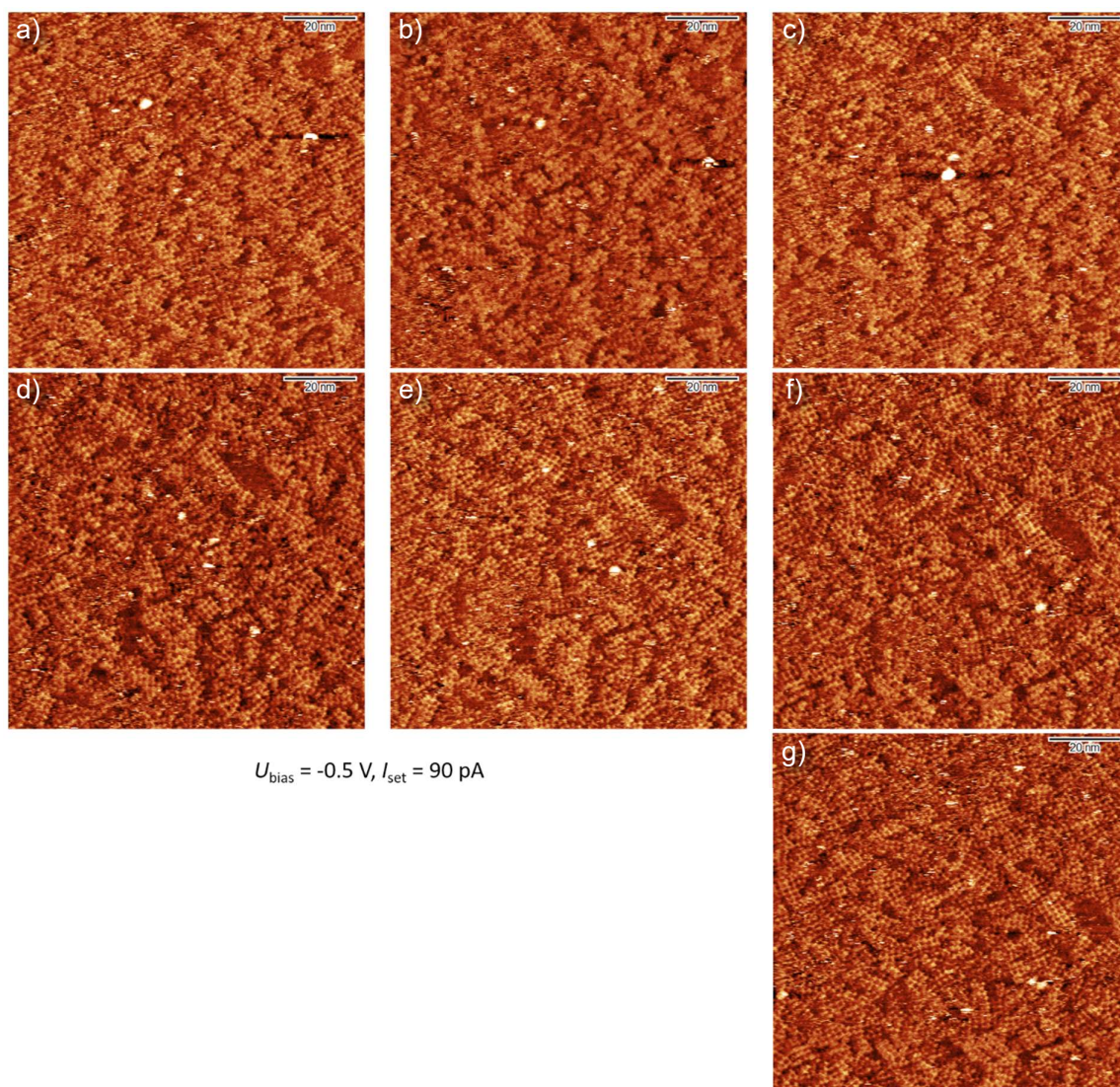


Fig. S5 Time-series of large-scale STM images of the 2-in-1 monomer at the OA-DMSO/HOPG interface, at room temperature. Concentration = $5 \times 10^{-5} \text{ M}$. The images were obtained over twelve minutes, with each image being scanned within approximately 90 s (from top left to bottom right). The scale bar equals 20 nm. Imaging parameters: $V_{\text{bias}} = -0.5 \text{ V}, I_{\text{set}} = 0.90 \text{ nA}$

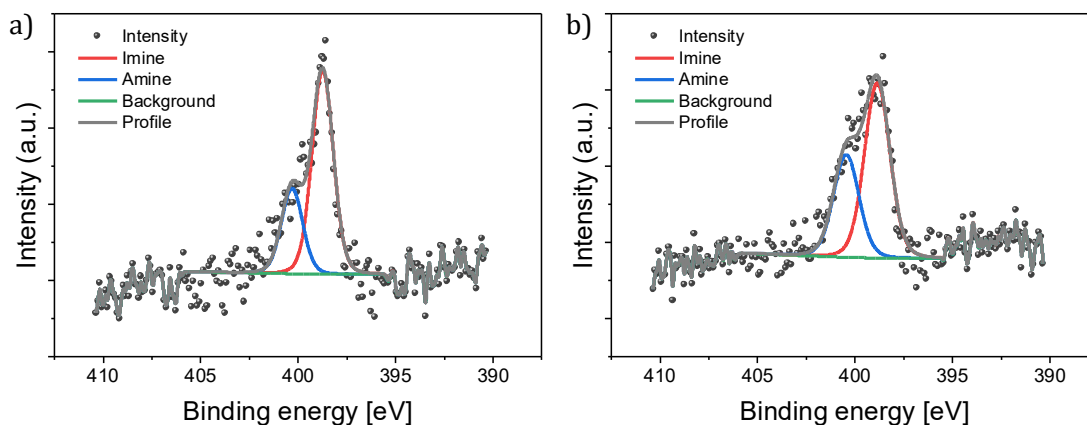
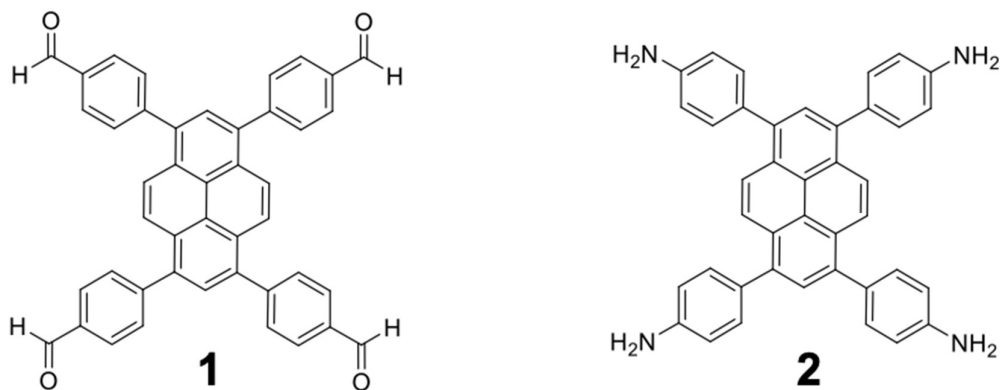


Fig. S6 Additional XPS data showing the influence of thorough rinsing for the removal of residual monomers from the sample. Two samples were rinsed using slightly different protocols. (a) XPS spectrum in $N1s$ region for a sample rinsed repeatedly using isopropanol. (b) XPS spectrum in $N1s$ region for a sample cleaned by intense washing in isopropanol (the HOPG sample was submerged in isopropanol and stirred for 15 min using a specially made rinsing vial which holds the sample in place while the solution is stirred. This spin cleaning vial allows thorough rinsing due to a solvent vortex created on the HOPG surface). The XPS spectra in both cases are fundamentally similar to that provided in the original text and still show the amine signal despite thorough rinsing. This indicates that the contribution to this signal largely comes from the edge of the flakes which is in line with small flake size as confirmed from the STM data.

STM versus XPS:

We calculated the imine/amine(+ammonium) ratio, which is $1:0.7 \pm 0.2$ for the sample washed vigorously with isopropanol. The ratio is low (given the fact that a single unit cell of the imine COF, consisting of four covalently connected molecules, would show a ratio of 1:1) and the standard deviation is very large. While the average domain sizes seen in the STM images is also small, the large variety in sizes and the multilayer appearance on the surface render an exact determination difficult. It must be noted that the surface area that is analysed in a single XPS scan is much larger than the $100 \cdot 100 \text{ nm}^2$ area typically scanned by the scanning tunnelling microscope. Thus, there can be large empty or sparsely populated areas contributing to the XPS signal which were not observed with STM. Additionally, the samples used for XPS were heated to dryness, while STM was performed at the liquid/solid interface. Thus, the nature of the sample used for XPS and STM is different, especially given the changed reaction rate at higher temperatures and the expected formation of much more layers of COF nanoflakes in the dry XPS sample.

We synthesised structurally similar tetraaldehyde (**1**) and tetraamine (**2**) in order to compare the 2D-COF formation with the results obtained on the 2-in-1 monomer. However, STM experiments carried out on the mixture of these two monomers did not reveal any network formation at the solution-solid interface. We ascribe this to the poor solubility of the tetraaldehyde **1** in common organic solvents.



Synthesis of 1,3,6,8-tetrakis(4-formylphenyl)pyrene (**1**)²

1,3,6,8-tetrabromopyrene (518 mg, 1.0 mmol), 4-formylphenylboronic acid (900 mg, 6.0 mmol), K_2CO_3 (566 mg, 7.0 mmol) and $Pd(PPh_3)_4$ (115 mg, 0.1 mmol) were refluxed at reflux in the mixture of 1,4-dioxane and H_2O ($V:V = 4:1$, 20 mL) for 3 d. After cooling to room temperature, the mixture was poured into ice water (50 mL). The precipitate was collected by filtration and was washed with H_2O and MeOH. The resulting yellow powder was dried under vacuum (410 mg, 67 %). 1H NMR (400 MHz, $CDCl_3$): 10.16 (s, 4 H), 8.18 (s, 4 H), 8.10 (d, 8 H), 8.04 (s, 2 H), 7.87 (d, 8 H).

Synthesis of 1,3,6,8-tetrakis(4-aminophenyl)pyrene (**2**)²

1,3,6,8-tetrabromopyrene (518 mg, 1.0 mmol), 4-aminophenylboronic acid pinacol ester (1320 mg, 6.0 mmol), K_2CO_3 (566 mg, 7.0 mmol) and $Pd(PPh_3)_4$ (115 mg, 0.1 mmol) were refluxed at reflux in the mixture of 1,4-dioxane and H_2O ($V:V = 4:1$, 20 mL) for 3 d. After cooling to room temperature, the mixture was poured into ice water (50 mL). The precipitate was collected by filtration and was washed with H_2O and MeOH, Recrystallization from 1,4-dioxane to afford yellow powder (450 mg, 80 %). 1H NMR (400 MHz, $DMSO-d_6$): δ (ppm) 8.11 (s, 4H), 7.77 (s, 2H), 7.34 (d, 8H), 6.76 (d, 8H), 5.32 (s, 8H).

References

1. Y. Li, Q. Chen, T. Xu, Z. Xie, J. Liu, X. Yu, S. Ma, T. Qin and L. Chen, *J. Am. Chem. Soc.*, **2019**, *141*, 13822–13828.
2. L. Ascherl, E. W. Evans, M. Hennemann, D. Di Nuzzo, A. G. Hufnagel, M. Beetz, R. H. Friend, T. Clark, T. Bein and Florian Auras, *Nat. Commun.* **2018**, *9*, 3802.
3. D. Nečas and P. Klapetek, *Cent. Eur. J. Phys.* **2012**, *10*, 181.